DOI 10.1007/s11182-021-02248-y
Russian Physics Journal, Vol. 63, No. 11, March, 2021 (Russian Original No. 11, November, 2020)

SERVICE LIFE EFFECT ON STRUCTURE AND PHASE COMPOSITION OF DIN 14MoV63 STEEL

N. A. Popova,[1] E. L. Nikonenko,[1,2] N. V. Ababkov,[3,4] A. N. Smirnov[3,4] UDC 620.18:620.16

The paper studies the structure and phase composition of steel 0.12C–1Cr–1Mo–1V–Fe *(grade DIN 14MoV63) after a long-term operation using the transmission electron microscopyю Investigated are the nontreated specimen (not subjected to operation) and specimens after a long-term operation with and without fracture. The phase composition and morphology of the steel structure are determined for each specimen. It is found that the steel servicing leads to the destruction of lamellar perlite, intensive fragmentation of ferrite, redistribution of the carbide component and elastic distortion of the crystal lattice.*

Keywords: steel, morphology, phase composition, ferrite, perlite, carbide particle, fine structure parameters.

INTRODUCTION

The problem of the material reliability in various structures remains relevant for many years. Recently, it has become more acute as a result of a decrease in the service life of structures due to the material degradation during its operation. This requires the material hardening and the elaboration of recommendations for extending its service life. This problem is now receiving more and more scientific attention. It is necessary to study the processes of the defect accumulation and identify the main fracture processes, because irreversible changes in the material structure during its long-term operation, can intensify the defect nucleation and accumulation. Moreover, the material structure modification increases the risk of early fracture, making it a necessity to evaluate the probability of fracture and to facilitate the relationship between the statistical characteristics and the fracture processes of the material. The structural safety precautions imply the preservation of mechanical properties of the material during its period of operation. However, the effective stress [1–6], corrosive environment [1, 7], cyclic loads [2, 8], residual stresses [9], temperature [10–13], defects arising during the operation [14] modify the mechanical properties of the material. The literature in the field mainly concerns the operation-induced changes in the mechanical properties. The material hardening and cracking during the operation substantially influenced by changes in the fine structure parameters, defect accumulation and internal stresses, remain largely unexplored. In this regard, the purpose of this work is to study the service life effect on the structure, phase composition and internal stresses in steel 0.12C-1Cr-1Mo-1V-Fe (grade DIN 14MoV63). The main attention is paid to the quantitative changes in the phase composition and fine structure of the steel.

MATERIALS AND METHODS

The steel 0.12C-1Cr-1Mo-1V-Fe (grade DIN 14MoV63) specimens were used to subject them to a long-term operation on 1) on the nontreated steel specimen (not subjected to operation), 2) after 263 000-hour operation without

[1]Tomsk State University of Architecture and Building, Tomsk, Russia, e-mail: natalya-popova-44@mail.ru; vilatomsk@mail.ru; [2]National Research Tomsk Polytechnic University, Tomsk, Russia; [3]Gorbachev Kuzbass State Technical University, Kemerovo, Russia, e-mail: n.ababkov@rambler.ru; [4]OOO 'Kuzbass Center for Welding and Control', Kemerovo, Russia, e-mail: galvas.kem@gmail.com. Translated from Izvestiya Vysshikh Uchebnykh Zavedenii, Fizika, No. 11, pp. 57–62, November, 2020. Original article submitted June 8, 2020.

TABLE 1. Chemical Compositoion of Steel Grade DIN 14MoV63, in wt.%

C	V	Si	Cu	Mo	Mn	Ni	Cr	P	S	Fe
0.08–1.15	0.15–0.30	0.17–0.37	≤0.20	0.25–0.35	0.40–0.70	≤0.30	0.90–1.20	≤0.025	≤0.025	Residues

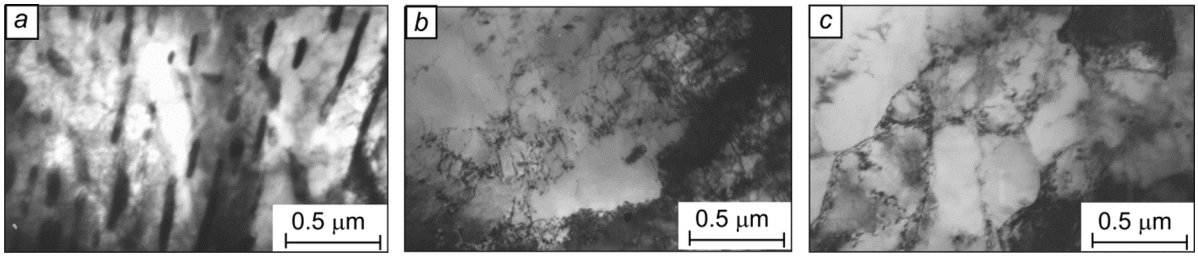

Fig. 1. TEM images of morphological components of DIN 14MoV63 steel specimens: *a* – lamellar perlite, *b* – nonfragmented ferrite, *c* – fragmented ferrite.

fracture, and 3) after 360 000-hour operation to fracture. The chemical compositoion of DIN 14MoV63 is presented in Table 1.

The structure and phase composition of the DIN 14MoV63 thin foils were studied on an EM-125 transmission electron microscope (TEM) at a 125 kV accelerating voltage. The optical viewing system magnification was 25000×. The phase morphology, composition, presented phases and their localization were classified for each specimen. The calculated parameters of the fine structure included the volume fraction P_V of the structural components; the density distribution and volume fractions of carbide particles; scalar and excess dislocation densities ρ and $\rho_{\pm}$; the bending-torsion amplitude χ of the crystal lattice; and the internal stress amplitude σ. The quantitative parameters of the fine structure were determined both for each structural component of the steel and in each specimen on a whole. The obtained data were statistically processed.

The phase composition was studied by using the TEM images, X-ray diffraction patterns and dark-field images obtained in the respective reflections. The linear size and scalar dislocation density were detected on micrographs using the secant method in accordance with the standard procedures. The excess dislocation density is $\rho_{\pm} = \rho_{+} - \rho_{-}$, where ρ_{+} and ρ_{-} are densities of positive and negative dislocations, respectively. It was measured by local misorientation or by the bending-torsion amplitude χ of the crystal lattice [15]. The latter was identified by the presence of bend extinction contours in the material, according to [15]. Two types of internal stresses were detected: 1) shear stresses (forest dislocation) created by the dislocation structure [16] and 2) long-range stresses localized in places with the excess dislocation density $\rho_{\pm}$, *viz*., at $\rho_{\pm} = \rho_{+} - \rho_{-} \neq 0$ [16].

PHASE COMPOSITION AND STRUCTURE OF NONTREATED STEEL

Phase composition

According to the results obtained, the steel matrix of the nontreated specimen represents the α-phase, which is a solid solution of carbon and alloying elements in the α-Fe phase with the body-centered cubic lattice. As can be seen from Fig. 1, the morphological components of the α-phase are lamellar perlite and ferrite. The volume fraction of lamellar perlite is 35%. It is present in the form of grains or grain aggregates, where cementite lamellas are found either partially or completely fractured (see Fig. 1*a*). The average particle size of cementite in perlite is 40×600 nm; the total volume fraction is 9.2%.

The ferrite grains are observed both in nonfragmented (Fig. 1*b*) and fragmented (Fig. 1*c*) strucutre. As is known from [15, 17, 18], the fragmented structure results from a deep rearrangement of the dislocation structure. Most of the fragment boundaries are misoriented grain boundaries, rather than dislocations.

TABLE 2. Average Quantitative Parameters of Fine Structure of Morphological Components in Nontreated Specimens of DIN 14MoV63 Steel

Morphological components	Quantitative parameters of the fine structure					
	Volume fraction P_V, %	Dislocation density ρ, cm^{-2}	Excess dislocation density $\rho_{\pm}$, cm^{-2}	Bending-torsion amplitude χ, cm^{-1}	Forest dislocation σ_f, MPa	Long-range stress σ_l, MPa
Perlite	35	$2.78 \cdot 10^{10}$	$1.28 \cdot 10^{10}$	320	335	225
Nonfragmented ferrite	30	$2.94 \cdot 10^{10}$	$1.64 \cdot 10^{10}$	410	340	255
Fragmented ferrite	35	$2.25 \cdot 10^{10}$	$1.78 \cdot 10^{10}$	445	300	265
Bulk material	100	$2.64 \cdot 10^{10}$	$1.56 \cdot 10^{10}$	390	325	250

The volume fraction of nonfragmented and fragmented ferrite is 30 and 35%, respectively. The nonfragmented ferrite grains is a mixture of ferrite and carbide, in particular, ~20 nm fine carbide particles of the type $M_{23}C_6$ are observed on dislocations inside grains. This carbide type has a face-centered cubic structure. Its volume fraction in nonfragmented ferrite is 0.38%.

The type $M_{23}C_6$ carbide particles are also present in fragmented ferrite, both inside and on the boundaries of the fragments. Carbide particles on dislocations inside the fragments have a round shape. The average size of carbide particles is similar to that in nonfragmented ferrite, but their volume fraction is 0.1%. Carbide particles locating on the boundaries between the fragments are coarser. Their average size and the volume fraction are 40 nm and 1.49%, respectively. And these parameters of carbide particles are significantly higher than those inside the fragments.

Dislocation structure and internal stresses

The dislocation structure both in perlite and ferrite (nonfragmented and inside the fragments) is a dense dislocation network. The values of the average scalar dislocation density ρ are given in Table 2. Although this parameter is almost similar for all the morphological components, the highest value belongs to nonfragmented ferrite and the lowest value has fragmented ferrite.

The α-phase of the nontreated specimen is characterized by the large bending-torsion amplitude χ of the crystal lattice, that is confirmed by the bend extinction contours observed in all morphological components [15]. According to Table 1, the perlite steel component demonstrates the lowest bending-torsion amplitude. In nonfragmented and fragmented ferrites this value is almost similar, but higher than in nonfragmented ferrite.

According to the results obtained, the bend extinction contours presenting in all morphological components do not relate to well-defined stress sources. Therefore, the bending-torsion amplitude χ in the nontreated steel specimen is rather associated with the intrinsic dislocation structure. Moreover, the data in Table 2 concerning the χ value, show that $\rho_{\pm} \geq 0.5\rho$ for all morphological components. The presence of $\rho_{\pm}$ parameter means that the dislocation structure is polarized (or charged) especially in localized regions. Polarization of the dislocation structure leads to the formation of long-range internal stresses [15], whose amplitude is also given in Table 2. It is important to note that such stresses occur only in localized regions created by the dislocation charge and do not cover the whole material.

As can be seen from Table 2, fragmented ferrite has the highest values of $\rho_{\pm}$ and σ_l. This implies that the dislocation structure inside the fragments is strongly polarized, i.e., most of dislocations presenting in the fragments are excess dislocations. The dislocation structure rearrangement observed during its formation, results in the significant annihilation of positive and negative dislocations inside each fragment while maintaining the excess dislocation density.

The amplitude of the internal shear stress produced by the forest dislocation σ_f is calculated using the dislocation density ρ [15]. These data summarized in Table 2.

Thus, the localized stress fields are provided by not only the intrinsic dislocation structure σ_f, but also the charged dislocation structure σ_l. According to Table 2, the lowest ρ and σ_f parameters belong to fragmented ferrite and the highest are observed in perlite. Nevertheless, the condition of $\rho > \rho_{\pm}$ and $\sigma_f > \sigma_l$ holds for both fragmented ferrite

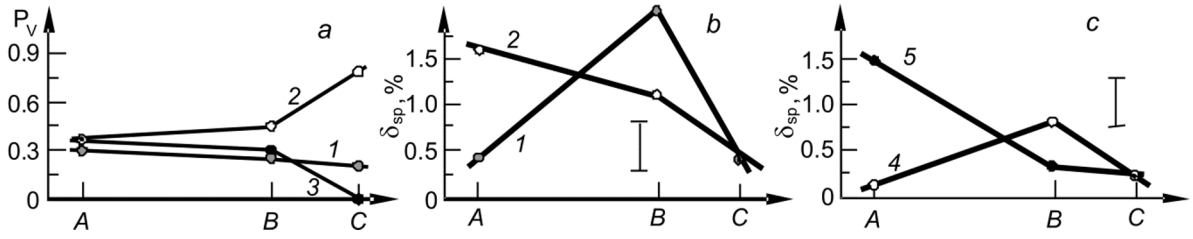

Fig. 2. Volume fraction P_V of different components in DIN 14MoV63 steel after long-term operation: *a* – morphological components, *b* – the type $M_{23}C_6$ (δ_{sp}) carbides inside morphological components, *c* – the type $M_{23}C_6$ (δ_{sp}) carbides inside and on the boundaries of fragmented ferrite; *1* – nonfragmented ferrite, *2* – fragmented ferrite, *3* – lamellar perlite, *4* – carbides inside fragments, *5* – carbides on fragment boundaries; *A* – nontreated steel specimen, *B* – specimen after long-term operation without fracture, *C* – specimen after long-term operation till fracture; sp stands for special carbides.

and the bulk material. This means that the crystal lattice distortion in the nontreated steel specimen is plastic and does not lead to the microcrack formation in the material [15].

STRUCTURE AND PHASE COMPOSITION OF DIN 14MoV63 STEEL AFTER LONG-TERM OPERATION

Phase composition

Our investigations show that that the service life of the DIN 14MoV63 steel does not modify the morphological components of the α-phase. Independently of the service time and/or conditions, lamellar perlite, nonfragmented and fragmented ferrite are present in the steel matrix in different amount. Nevertheless, the morphological components in the nontreated steel specimen are shared equally, whereas during the long-term operation to fracture, this ratio changes such that lamellar perlite gradually disappears (disintegrates) and is not then detected at all (see Fig. 2*a*). Fragmented ferrite prevails in the steel matrix after the long-term operation.

The size, density distribution, and volume fraction of carbide particles in the carbide subsystem change after the long-term operation of the DIN 14MoV63 steel, the particle shape being unchanged. In perlite, the cementite particles change their size and density distribution. At the same time, the decrease in the longitudinal size is more intensive than the transverse. This indicates that during the long-term operation, the cementite particles are grinded by slip dislocations [19] and dissolved by the motion of carbon atom from carbide phase (cementite) onto the crystal lattice defects of ferrite [20].

As noted above, the nontreated steel specimen with nonfragmented ferrite is characterized by the presence of the type $M_{23}C_6$ carbide particles. At the beginning of the long-term operation, carbide particles are coagulated, since their size grows and the density of distribution lowers. Then, similar to cementite, carbide particles dissolve due to the carbon atom transfer to the crystal lattice defects of ferrite. This is proven by the decrease in the particle size and the density of distribution. According to Fig. 2*b* (curve *1*), the volume fraction of this phase increases and then decreases.

The nontreated steel specimen with fragmented ferrite is characterized by the type $M_{23}C_6$ carbide particles mostly concentrating on the fragment boundaries; inside the fragments the volume fraction of this phase is low (see Fig. 2*c*). The long-term operation of the steel specimens provides the same effect on the volume fraction of this phase inside the fragments as in nonfragmented ferrite. As illustrated in Fig. 2*c* (curve *4*), the volume fraction of the carbide phase grows and then lowers. On the fragment boundaries, $M_{23}C_6$ particles dissolve, i.e., their size and the distribution density decrease. The volume fraction of carbides also lowers, as shown in Fig. 2*c* (curve *5*), whereas it is identical both in the fractured specimen (Fig. 2*c*, point *C*) and at the fragment boundaries. The total volume fraction of the type $M_{23}C_6$ carbide particles in fragmented ferrite decreases with increasing time of operation (see Fig. 2*b*, curve *2*).

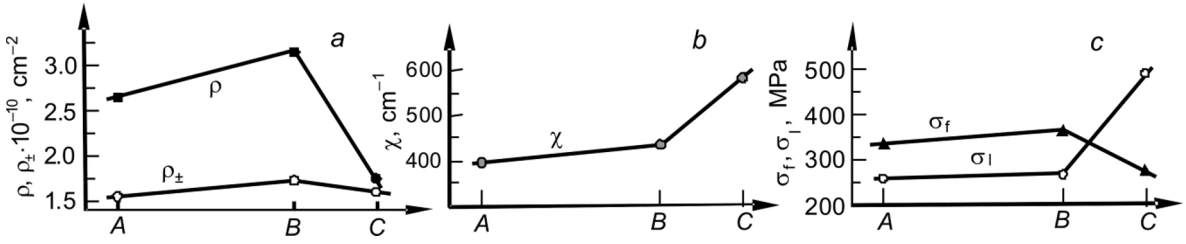

Fig. 3. Changes in the DIN 14MoV63 steel with increasing operation time: *a* – scalar (ρ) and excess ($\rho_{\pm}$) dislocation densities; *b* – bending-torsion amplitude χ of the crystal lattice; *c* – internal stress amplitudes (σ_f stress induced by the dislocation structure and σ_l localized stress). *A* – nontreated steel specimen, *B* – specimen after long-term operation without fracture, *C* – specimen after long-term operation till fracture.

Dislocation structure and internal stresses

The dislocation structure in the bulk material as well as in the nontreated specimen, represents a dense dislocation network. Initially, the long-term operation of steel specimens leads to an increase in the scalar dislocation density and then to its decrease both in each morphological component and in the bulk material. As shown in Fig. 3*a*, the values of scalar and excess dislocation densities gradually become closer and coincide in the fractured specimen. This indicates that all dislocations in the material are excess dislocations.

At the initial stage, the long-term operation weakly affects the bending-torsion amplitude of the crystal lattice in all morphological components. But later it causes a dramatic increase in this parameter in fragmented ferrite, which is explained by the formation of the elastic component χ_{el}. The bending-torsion amplitude of the crystal lattice in fragmented ferrite is calculated as $\chi = \chi_{pl} + \chi_{el}$. As the volume fraction of fragmented ferrite after the long-term operation to fracture is ~80% of the steel matrix, the bending-torsion amplitude χ dramatically grows (see Fig. 3*b*) and is also $\chi_{pl} + \chi_{el}$. The value of χ_{pl} is 2.5 times higher than χ_{el} value. As a result, the amplitude of the localized stress σ_l, fully determined by χ, also equals $\sigma_l = \sigma_l^{pl} + \sigma_l^{el}$ and is 1.8 times higher than the internal shear stress σ_f, which is determined by the dislocation structure (Fig. 3*c*) and causes the specimen disintegration.

CONCLUSIONS

Based on the TEM observations, it was found that the long-term operation of the steel specimens led, first, to the destruction of lamellar perlite and the intensive fragmentation of ferrite. Second, it caused a complete destruction of cementite and the redistribution and destruction of the type $M_{23}C_6$ carbides and, third, to the elastic distortion of the crystal lattice.

This work was carried out within the government contract N FEMN-2020-0004 and financially supported by the Grant N MK-1084.2020.8 from the President of the Russian Federation.

REFERENCES

1. I. R. Kuzeev, G. E. Zakirnichnyi, and L. F. Zakirova, Met. Sci. Heat Treat., **51**, No. 9–10, 450–453 (2009).
2. L. R. Botvina, V. G. Budueva, A. A. Ostapenko, *et al*., Deformatsiya i razrushenie materialov, No. 12, 28–35 (2013).
3. L. R. Botvina, Yu. A. Demina, I. M. Petrova, *et al*., Mashinostroenie i inzhenernoe obrazovanie, No. 4(45), 27–34 2015.

4. A. S. Syromyatnikova, E. M. Gulyaeva, and K. I. Alekseeva, Russian metallurgy (Metally), No. 10, 996–998 (2017).
5. E. A. Tikhomirova, A. I. Rybnikov, and L. B. Getsov, Met. Sci. Heat Treat., **59**, No. 1–2, 34–38 (2017).
6. M. V. Demchenko and I. R. Kuzeev, Nanotekhnologii v stroitel'stve, **10**, No. 4, 39–56 (2018).
7. G. V. Pachurin, N. A. Kuz'min, D. A. Goncharova, *et al*., Sborka v mashinostroenii, priborostroenii, No. 9, 396–401 (2019).
8. I. M. Petrova, I. V. Gadolina, L. R. Botvina, *et al*., Zav. lab. Diagnostika materialov, **77**, No. 1, 58–61 (2011).
9. G. N. Nikiforchin, O. T. Tsirul'nik, O. I. Zvirko, *et al*., Zav. lab. Diagnostika materialov, **79**, No. 9, 48–55 (2013).
10. I. V. Gorynin and B. T. Timofeev, Voprosy materialovedeniya, No. 1(65), 41–59 (2011).
11. V. M. Konstantinov, E. P. Puchkov, and A. I. Galimskii, Polzunovskii al'manakh, No. 2, 41–44 (2014).
12. G. V. Pachurin, Fundamental'nye issledovaniya, No. 1, 18–23 (2014).
13. Getsov L., Rybnikov A., Semenov A., *et al*., Mater. Tehnol., **49**, No. 5, 773–778 (2015).
14. I. I. Kryukov, A. I. Rybnikov, N. V. Mozhaiskaya, *et al*., Gazoturbinnye tekhnologii, No. 2(129), 32–37 (2015).
15. N. A. Koneva and E. V. Kozlov, Russ. Phys. J., **34**, No. 3, 224–236 (1991).
16. M. A. Shtremel, Strength of Alloys. Lattice Defects [in Russian], Metallurgiya, Moscow (1982).
17. E. V. Kozlov, N. A. Popova, O. V. Kabanina, *et al*., Evolution of Phase Composition, Defect Structure, Internal Stresses and Carbon Redistribution During Structural Steel Casting [in Russian], SibGIU, Novokuznetsk (2007).
18. E. V. Kozlov, N. A. Popova, and N. A. Koneva, Bull. Russ. Acad. Sci. Phys., **68**, No. 10, 1587–1560 (2004).
19. M. V. Belous, M. A. Vasil'ev, A. A. Kosyachkov, *et al*., Metallofiz., **4**, No. 2, 86–91 (1982).
20. V. G. Gavrilyuk, Carbon Distribution in Steel [in Russian], Naukova dumka, Kiev (1987).